Physica Medica 136 (2025) 105017

Contents lists available at ScienceDirect

Physica Medica

journal homepage: www.elsevier.com/locate/ejmp

Original paper

Patient-specific organ dose and *in-vivo* image quality assessment in clinical CT

Wanyi Fu [a,1,*], Shobhit Sharma [b,2], Justin Solomon [c], Francesco Ria [c], Hananiel Setiawan [d], Aiping Ding [e], William P. Segars [f], Ehsan Samei [g]

[a] Center for Virtual Imaging Trials, Carl E. Ravin Advanced Imaging Labs, and Department of Electrical and Computer Engineering, Duke University, Durham, NC 27708, USA

[b] Center for Virtual Imaging Trials, Carl E. Ravin Advanced Imaging Labs, and Medical Physics Graduate Program Duke University, Durham, NC 27708, USA

[c] Center for Virtual Imaging Trials, Carl E. Ravin Advanced Imaging Labs, Clinical Imaging Physics Group, Duke University Health System, Durham, NC 27710, USA

[d] Center for Virtual Imaging Trials, Carl E. Ravin Advanced Imaging, Medical Physics Graduate Program, Duke University, Durham, NC 27708, USA

[e] Clinical Imaging Physics Group, Duke University Health System, Durham, NC 27710, USA

[f] Center for Virtual Imaging Trials, Carl E. Ravin Advanced Imaging, Departments of Radiology and Biomedical Engineering, Duke University, Durham, NC 27708, USA

[g] Center for Virtual Imaging Trials, Carl E. Ravin Advanced Imaging Labs, Clinical Imaging Physics Group, Medical Physics Graduate Program, Departments of Radiology, Electrical and Computer Engineering, Biomedical Engineering, and Physics, Duke University, Durham, NC 27708, USA

ARTICLE INFO

Keywords:
Computed tomography
organ dose
Quality control
computational phantom
Monte Carlo

ABSTRACT

Purpose: To develop and characterize individualized dose and quality measures at organ level compared to their generic counterparts across a clinical CT dataset.

Materials and methods: The study included 9801 chest-abdomen-pelvis and abdomen-pelvis CT exams (7,763 patients, mean age, 56 ± 17 years; 4113 women) representing 20 unique protocols. For each exam, patient-specific organ dose of all radiosensitive organs was estimated using a validated method by generating personalized computational phantoms and Monte Carlo simulations. Effective dose (E_{OD}) was calculated by weighted sum of the organ doses. Liver dose, OD_{liver}, noise in the liver, N_{liver}, and observer model detectability, d', were assessed within the liver as examples of individualized, organ-based image assessment measurements. The organ-based measurements (OD_{liver}, E_{OD}, and N_{liver}) were compared to their generic counterparts: ssize-specific ddose estimates (SSDE), effective dose based on dose length product (E_{DLP}), and whole-body noise (N_{global}), respectively.

Results: Generic dose values were substantially higher than individualized estimates for SSDE vs. OD_{liver} (median of all exams: 51.2 %, $p < 0.001$) and E_{DLP} vs. ED_{OD} (median: 41.0 %, $p < 0.001$). N_{global} was generally lower than N_{liver} (median: −7.2 %, $p < 0.001$). The correlation relationships of E_{OD} and d' were substantially varied (R^2 range: 0–0.5) for different patient sizes and scan parameters.

Conclusions: Demonstrated across a population of exams, individualized organ-based measurements of dose and quality are feasible. Generic measures cannot fully represent individualized organ-based values. The correlation relationships between individualized dose and image quality values varies for different vendors and protocols, implying imaging optimization is best when done semi-independently for each factor using individualized measurements.

1. Introduction

While computed tomography (CT) continue to provide an undisputed clinical value [1], in practice, CT image quality and associated radiation doses vary substantially for a given exam type due to the differences in patient attributes and scan settings [2]. As medicine is ultimately about patient care, accurate and patient-centered assessment of radiation dose and image quality can provide more relevant reflection of

* Corresponding author.

E-mail addresses: wanyifu@tsinghua.edu.cn (W. Fu), shsharma@mru.medical.canon (S. Sharma), justin.solomon@duke.edu (J. Solomon), francesco.ria@duke.edu (F. Ria), hananiel.setiawan@duke.edu (H. Setiawan), aiping.ding@duke.edu (A. Ding), paul.segars@duke.edu (W.P. Segars), ehsan.samei@duke.edu (E. Samei).

[1] Present address: Department of Electronic Engineering, Tsinghua University, Beijing 100084, China.

[2] Present address: Canon Medical Research USA, 706 Deerpath Dr, Vernon Hills, IL 60061, USA.

https://doi.org/10.1016/j.ejmp.2025.105017
Received 8 February 2025; Received in revised form 14 April 2025; Accepted 25 May 2025

this variability to improve consistency and to ensure sufficient image quality at appropriate radiation dose [3–5]. Such individualized data can further help to evaluate the relationships between radiation dose, image quality, patient attributes, and scan parameters *in vivo*; and to inform the design and optimization of the technology in view of its clinical output.

In clinical practice, patient radiation dose is often represented by surrogates such as size-specific dose estimates (SSDE), which incorporate the volume CT dose index ($CTDI_{vol}$) with patient-size adjustment [6–8]. Further, effective dose based on the dose length product (E_{DLP}), though originally defined for reference dose estimation, is commonly used to reflect the overall exposure of a given scan [3; 7; 9]. However, both SSDE and E_{DLP} quantify dose from idealized models, instead of accounting for individual patient anatomies with unique geometries and organ-specific radiation sensitivities [10]. Moreover, these metrics do not reflect dose dependencies to personalized dose reduction techniques such as tube current modulation, which are routinely used in modern clinical practice [11]. In contrast, patient-specific organ dose and organ dose-based effective dose (E_{OD}), calculated as the weighted sum of organ dose, offer more clinically relevant metrics to quantify patient radiation burden [4,12]. Organ doses can be precisely estimated using patient-specific computational models and exam-specific radiation field. However, achieving accurate dose modeling in clinical settings remains challenging due to variability in patient anatomy, scanners, and protocols [10].

More important than radiation dose, image quality is vital for imaging justification and optimization as it represents the effectiveness of an image to provide for a diagnostic task [13]. Clinical image quality is often assessed either qualitatively or via a multi-observer study [14]. These approaches are either too subjective, or infeasible for practical clinical optimization. Alternative *in vivo* measures on patient images have recently been demonstrated feasible [15]. As diagnostic tasks typically take place at the organ level, such measures are most relevant at the organ level.

The purpose of this study was to estimate patient-specific organ dose and image quality automatically across a population of chest-abdomin-pelvis (CAP) and abdomen-pelvis (AP) CT studies with different scan parameters. The data were used to assess inherent variabilities and assess differing conclusions that may be drawn from such individualized, organ-based measures in contrast to those from generic measurements of radiation dose and image quality.

2. Materials and methods

This retrospective, HIPAA compliant study had been approved by the Institutional Review Board with waived informed consent.

2.1. CT scan protocols and series selection

A total of 9,801 CT exams from 7763 patients (mean age, 56 ± 17 years; 4,113 women) from March 24, 2015 to Dec 30th, 2017 were randomly selected out of 10,625 exams based on sufficient image volume and completeness of scan parameter information. The data were from five scanner models (SOMATOM Definition Flash and SOMATOM Force of Siemens Healthineers, Erlangen Germany; and LightSpeed VCT, Discovery CT750 HD, and Revolution CT of GE Healthcare, Waukesha, WI). For each exam, one primary axial series with slice thickness closest to 3 mm was selected to reflect diagnostic preference at our institution. Exams were grouped so that each group used a unique combination of scan settings of scanner model, bowtie filtration, beam collimation, pitch, kV, reconstruction algorithm, and slice thickness resulting in 20 different condition groups (Table 1). All exams were contrast enhanced scans.

Table 1
Summary of scan parameters and patient age and gender.

Manufact	LightSpeed VCT, Discovery CT750 HD, Revolution CT	SOMATOM Definition Flash, SOMATOM Force
Filter type	Body Filter	Wedge3, Wedge3/Sn, Flat
Collimation (mm)	40	38.4
Pitch	0.992 1.375	0.8
KVP	120, 140	90, 100, 110, 120, 140, 100/140
Reconstruction algorithm	FBP Standard, FBP Detail	SAFIRE-2 I31f, ADMIRE-2 Br40d
Slice thickness (mm)	2.5, 5	3, 5
CTDIvol (mGy)	12. 0 ± 5.9	
DLP (mGy-cm)	654.0 ± 330.3	
Patient Age (mean ± SD)	55 ± 18	57 ± 17
Number of patients	4047 (2217 women)	4481 (2310 women)

Note – Twenty different sets of scan parameters were evaluated in this study. Some patients were scanned by multiple exams both from vendor A and vendor B.

2.2. Image assessment

The CT studies were assessed by individualized organ dose, E_{OD}, noise, and *d'* (detailed below). The flowchart for individualized organ-based assessment is shown in Fig. 1.

2.3. Patient-specific organ dose

For each CT exam, patient-specific computational phantoms (virtual patient) were generated adapting a previously-developed framework [16]. Specifically, based on CT images, relatively distinguishable organs and structures were segmented using a Unet-based multi-organ segmentation model [17]. The segmented anatomies were used as an initial target for other unsegmented radiosensitive organs to be filled-in deformably from an anatomical template from a library of adult XCAT phantoms matched according to sex, height, and effective diameter. A diffeomorphic transformation was calculated between the XCAT and the initial patient target [18]. The resulting diffeomorphic field applied to the template filled in unsegmented radiosensitive organs resulting in a complete model of the patient.

The organ dose was estimated using a validated Monte Carlo program [19]. The program explicitly modeled the exam-specific scanner geometry, bowtie filtration, spectrum, and scan protocols including beam collimation and pitch. The angular tube current was synthesized using a scanner-specific technique [20]. In detail, patient attenuation was estimated using the CT images for anterior-posterior and lateral projections, which were used to interpolate a normalized tube current for all projection angles. Finally, the tube current values were calibrated to match the DICOM header value 'XrayTubeCurrent' in each slice. The combined use of the patient-specific phantom (i.e., generated by segmentation and diffeomorphic deformation) and the matched whole-body template enabled estimating doses to organs both within and outside the scan field of view. Based on the patient-specific organ doses, the E_{OD} was calculated as the weighted sum of the organ dose using tissue weighting coefficients from the ICRP Publication 103 [21]. As a comparison, E_{DLP} was calculated as the product of DLP and conversion coefficients ($k = 0.015$) according to ICRP Publication 102 [9].

2.4. In vivo organ-based image quality assessment

In this study, organ-based image quality was focused on the liver, one of the most common diagnostic targets in abdominal CT. For each exam, the liver region was automatically segmented from CT images using our organ segmentation model [22]. Noise was estimated for both the entire CT volume (N_{global}) and within the liver region (N_{liver}) using a validated

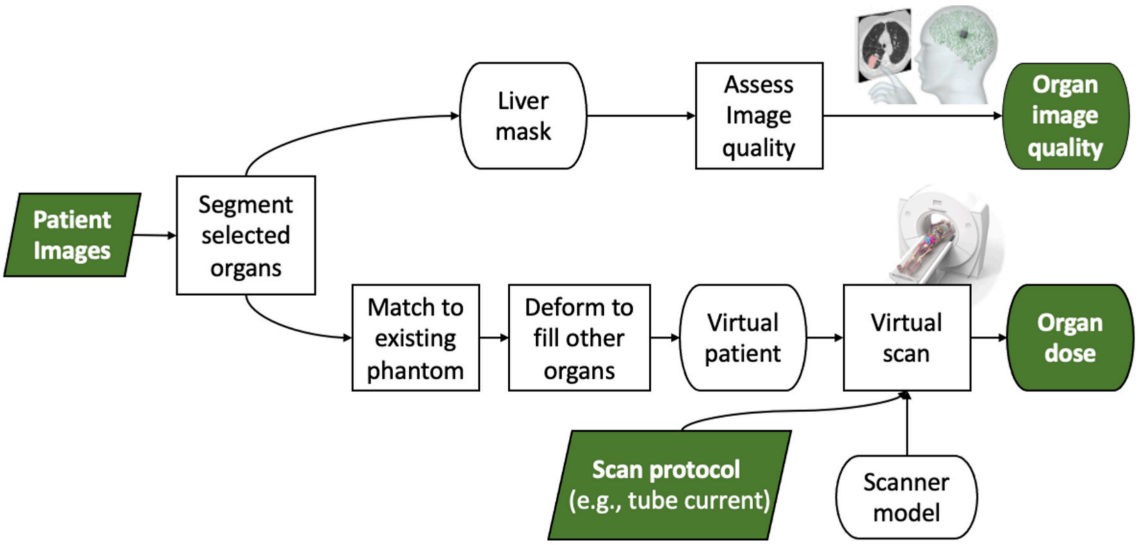

Fig. 1. Flowchart of individualized organ-based radiation dose and *in vivo* image quality assessment.

algorithm [23]. Specifically, the CT images were thresholded to remove high contrast features. Then standard deviation filters were applied, and the mode of the standard deviation value was used as the image noise. The liver detectability index (*d'*) was estimated using a non-pre-whitening observer model for a reference task of detecting a lesion with a 15 Hounsfield unit (HU) contrast and 5 mm diameter as a function of the noise power spectrum (NPS), modulation transfer function (MTF), and detection task [15]. NPS for d' calculation was estimated from patient CT images using a previously validated approach [15]. First, patient-specific noise magnitude was calculated using the same method as for Nliver and Nglobal .Scan-specific NPS shapes were selected from a library of prior measurements acquired using a Mercury phantom (Duke University), matched to each scan based on scan parameters [24]. The NPS was then calculated by scaling the selected NPS shape with the variance of the measured noise. The MTF was calculated based on the edge spread function from patient image air-skin boundaries [25].

2.5. Data analysis

The individualized organ-based measurements for CT exams across different scan settings were compared with their generic counterparts: liver dose versus SSDE, E_{OD} versus E_{DLP}, and N_{liver} versus N_{global} via 1) linear regression resulting in R^2, slope, intercept, and root mean square error of the fit (NRMSE), 2) percentage difference at median, 25th percentile (Q1), and 75th percentile (Q3), and 3) a paired *t*-test.

2.6. Clinical applications

To evaluate the utility of the metrology for clinical application, the organ-based metrics were applied to three common clinical scenarios. The first scenario was to determine diagnostic reference levels and variabilities of radiation dose. The median and interquartile (Q1-Q3) were estimated for liver dose, SSDE, E_{DLP}, and E_{OD} for patients with different ranges of water equivalent diameter (WED)[7]. The WED ranges (21–24.9 cm, 25–28.9 cm, 29–32.9 cm, 33–36.9 cm, 37–40.9 cm) were adopted from previous studies [26]. The second scenario was to identify outlier exams with large radiation dose and noise above 99th percentile thresholds. In the third scenario, the range of values and the relationships between E_{OD} and *d'*, reflecting the overall radiation risk and diagnostic performance of a diagnostic task, were estimated for patients with different WED ranges to determine the relationships between dose, image quality, and patient sizes across different scan settings. The median and 75th percentile of *d'* and E_{OD} were estimated across all exams, exams group by the scan parameters, and exams further grouped by WED ranges. Note that *d'* was estimated for both CAP and AP protocols together; while E_{OD} was estimated separately, as the latter can be affected by the scan coverage alone. Additionally, analysis of variance (ANOVA) was performed among exams with different WED ranges within the same scan setting group.

3. Results

3.1. Comparison of organ-based and non-organ-based dose measurements

In terms of dose, the generic, non-organ-based metrics were higher compared to the individualized, organ-based metrics (Fig. 2a and 2b). The SSDE were larger than OD_{liver} by a median of 51.2 % (Q1-Q3: 32.7–70.75 %, $p < 0.001$) estimated across all exams; the median values for each exam group ranged from 14.9-82.8 % ($p < 0.001$ for all groups). The higher values were also observed in the SSDE vs. OD_{liver} linear fits with positive intercept for all 20 groups (median 1.1 mGy; range 5.2–13.4 mGy). The group-wise R^2 showed a median of 0.65 (range 0.2–0.8); the slopes showed a median of 1 (range 0.6–1.3); the NRMSE showed a median of 1.8 mGy (1.2–3 mGy). Likewise, E_{DLP} was higher than E_{OD} ($p < 0.001$) for all exams except for a few cases with relatively low dose values. The median percentage differences between E_{DLP} vs. E_{OD} was 41 % (Q1-Q3 21.2–65.6 %) across all exams and ranged from 19.8 % to 107.9 % across all groups ($p < 0.001$ for all groups). The E_{DLP} vs. E_{OD} linear fits in each group showed a median R^2 of 0.60 (range 0.38–0.89), a slope of 1.5 (range 1.1–2.0), intercept of −0.1 mSv (range −3.2–8.4 mSv), and NRMSE of 1.8 mSv (range 0.88–4.5 mSv).

3.2. Comparison of organ-based and non-organ-based noise assessment

The N_{global} was found to be mostly lower than N_{liver} by median percentage differences of −7.2 % (Q1-Q3 −16.5–1.1 %) for all exams and ranged from −1% to −17.4 % across all 20 groups ($p < 0.001$ for all groups, Fig. 2c). The linear fits of N_{global} vs. N_{liver} showed slopes < 1 for all groups. The linear fits varied for different groups with an R^2 range of 0–0.8, slopes range of 0–0.9, intercept range of −0.9–12.5 HU, and the NRMSE range of 0.9–2 HU.

3.3. Clinical applications

The diagnostic reference levels and variabilities were significantly

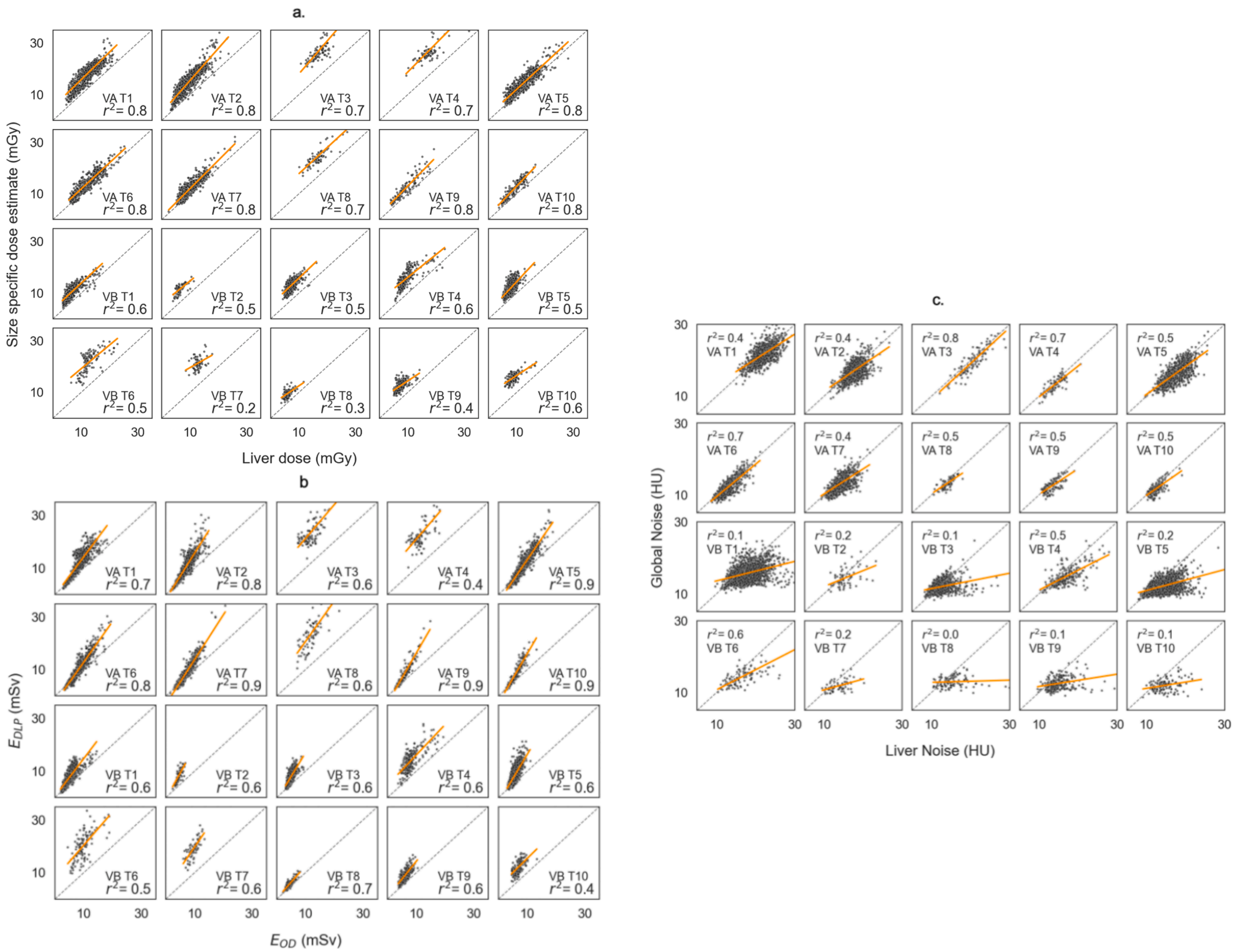

Fig. 2. Linear regression plots of non-organ-based vs. organ-based metrics in terms of *size specific dose estimate* vs. *liver dose* (a), in terms of *effective dose based on dose length product* (E_{DLP}) vs. *effective dose based on organ dose* (E_{OD}) (b), and in terms of *global noise* vs. *liver noise* (c). Each subplot shows exams with scan parameters VA T1 to VB T10 (VA or VB represent vendors; T represents techniques). Each data point is one exam measurement plotted with a linear regression line (solid orange line) and identical line (black dashed line).

different between organ-based and non-organ-based radiation dose estimates (Fig. 3). Further, the exam outliers with either high value for dose or noise were not identical using organ-based and non-organ-based measurements. When both organ-based and non-organ based metrics were used, the number of outlier exams in terms of liver dose, effective dose, and noise were 150, 151, and 167, respectively, but a third of those (namely 52, 52, and 69, respectively) were not identified as outlier if only non-organ-based metrics were used.

The median and 75th percentile of E_{OD} and d' for each sized-group, protocol-group, and across all exams are shown in Table 2. Fig. 4a and 4b show scatter plots of E_{OD} vs. d' along with their histograms for different patient sizes and scan parameters for CAP and AP scans, respectively. In general, E_{OD} and d' value-range and their relationships for different WED ranges substantially varied for different CT vendors. For example, with increasing WEDs, E_{OD} moderately increased for vendor A but largely remained unchanged for vendor B; d' increased for vendor A but slightly decreased for vendor B. A few cases with relatively small or large WED from vendor A showed an opposite trend. With increasing E_{OD}, d' moderately increased for vendor A (R^2 range 0–0.5) but maintained or slightly decreased for vendor B (R^2 range: 0–0.2). Overall, the relationships between E_{OD}, d', and WED substantially varied for different scan settings.

4. Discussion

The expanding usage of CT necessitates clinical safety and quality assessment in a relevant, informative, and patient-centric manner. Despite the recent development of patient-based and task-based protocol optimization techniques, the assessment of such tasks still relies exclusively on scanner output-based and phantom- or global-based indices (i.e., $CTDI_{vol}$, global noise, etc.). These indices are powerful but clearly the radiation dose and image quality measures can be more individualized at the organ level where imaging tasks commonly take place. In this study, we assessed images with scan-specific, patient-specific, and organ-based dose and image quality measurements for a population of exams across 20 scan techniques. The data were compared with their non-organ-based counterparts to assess their value and utility.

The study demonstrated that the generic dose and quality measures cannot fully represent their reflection at the level of an individual values ($p < 0.001$); these measures are most meaningfully characterized *in vivo* at individual organ levels and optimized as semi-independents attributes of the exam. Specifically, E_{DLP} was higher than E_{OD} by as much as 109 % (0.95 quantile), consistent with previous studies [27,28]. Furthermore, SSDE was higher than liver dose by as large as 103.9 % (0.95 quantile), consistent with a recent study [8]. Moreover, global noise was lower compared to liver noise. This is expected as global noise is dominated by

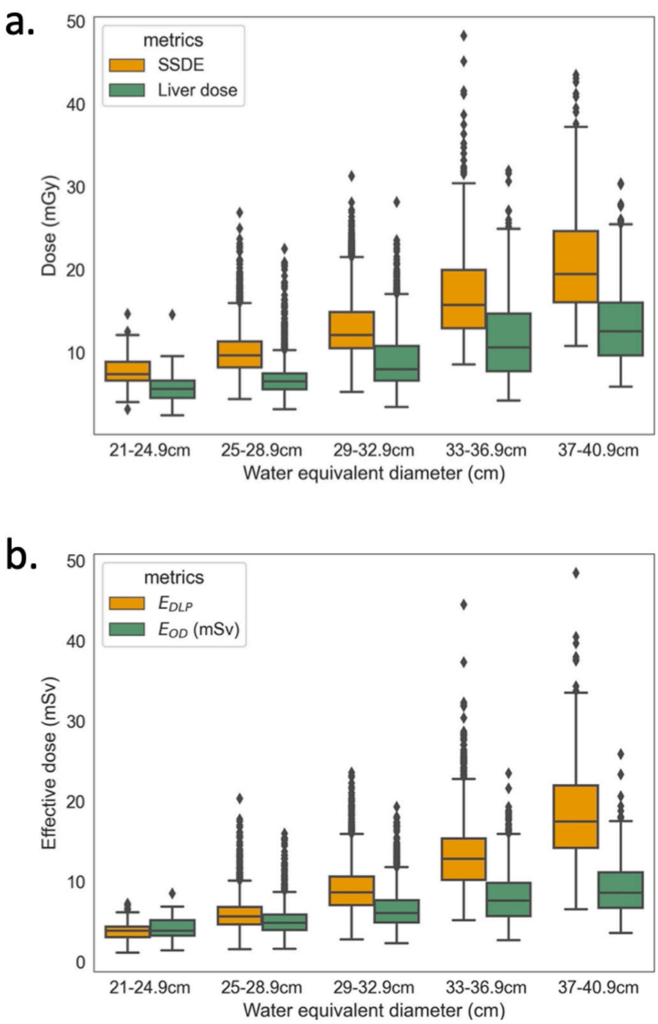

Fig. 3. Box plot of non-organ based and organ based metrics across different water equivalent diameter ranges across all exams for a. size-specific dose estimates (SSDE) and liver dose, b. effective dose based on organ dose (E_{OD}) and dose length product (E_{DLP}).

fat or muscle regions that have a different noise profile. Overall, the differences indicate that more specific surrogates of radiation dose and image quality are needed to better represent the individualized, organ-based radiation burden and diagnostic qualities.

The patient dose (E_{OD}) and image quality (d') value ranges varied significantly for different patient sizes and scan settings ($p < 0.001$). Although ideally, clinical exams show consistent quality across different patient anatomies, our results (Fig. 3) instead show substantial variations due to different interplay of differing scanners and patients. The presented methodology offers unique patient-specific data to precisely characterize clinical images and to inform protocol design targeting consistent and optimum clinical practice.

Generic image assessment measures as opposed to individualized one can lead to differing conclusions about a practice. For example, the variability in radiation dose was assessed to be 10.8–29.6 mSv (5th-95th percentile) when done based on ED_{DLP} for large-sized (WED: 37–40.9 cm) patients compared to 4.8–15.3 mSv based on ED_{OD}. Likewise, the radiation dose versus image quality showed differing results for generic vs. individualized data. Generic data, usually based on uniform phantoms resulting in unrepresentatively consistent CT radiation and reconstruction output, showed strong correlation between dose and image quality [29]. However, a patient triggers modulated radiation output, and adaptive reconstruction algorithms, which further interact with heterogeneous anatomies effecting the individualized measures. As such, the correlation between individualized organ-based dose and image quality was found to be dependent on the vendors and protocols. As observed, patients with equal dose showed a wide range of possible image quality values and vice versa. This implies image quality cannot be strongly predicted with increasing or decreasing dose as often assumed. These implies that targeting acceptable ranges of image quality may best be done in a semi-independent and individualized manner using patient-specific measurements.

We did not include a targeted assessment of errors of the measurands themselves. An earlier study [30] notes that such uncertainties are notably small. These variations are mainly originated from individual components adapted in this study. Specifically, for segmentation, across the 50 XCAT phantoms, the liver dose and effective dose showed differences of 1.4 ± 1.2 % and 2.7 ± 0.5 % compared to those using phantoms generated by the iPhantom framework and manual reference approaches [16]. The noise assessment showed discrepancies of 4.7 % compared to observer measurements, lower than reported multi-observer variabilities [23]. The patient-specific d' showed RMSE of 2.7 % and 2.3 % for images reconstructed using filtered back projection and iterative reconstruction, respectively.

The correlation coefficients of liver d' and E_{OD} were calculated to reflect the relationship between the performance of a typical diagnostic task and overall radiation risk. As an additional comparison, the correlation relationship between d' and liver dose was calculated. Compared to R^2 between d' and E_{OD}, R^2 between d' and liver dose was about 0.1 higher for scans from Vendor A and similar for scans from Vencor B for most of the protocols, with similar trends. The results indicate that the relationship between dose and image quality varies for different vendors and protocols.

This study has certain limitations. First, the study only included two vendors, one institution, and an adult population. The same methodology can be applied to other vendors, institutions, or pediatric cohort. Second, the assessment involved automated organ segmentation. The feasibility and generalizability of segmentation models were investigated in a previous study [22]. Organ dose and image quality reflect mean or median values within a voxelized organ volume; thus, automation proved sufficient in this study. Third, we demonstrated patient safety and quality assessment with limited metrics. However, the assessments are portable to other customized metrics such as patient risk or other diagnostic tasks in other organs. Forth, d' was calculated using an identical 15 HU lesion and a consistent contrast enhancement among all patients. Further study may consider the differences of patient contrast enhancement in determining image quality. Fifth, recent studies have shown that the presence of iodine contrast agents may increase dose to organ volumes. The findings by Mazloumi et al. reported that accounting for iodine in dose assessments in abdominal CT scans resulted in a 20–40 % increase in absorbed dose to key organs within the scan coverage [31]. In our work, organ dose was defined as the absorbed dose by tissue within each organ, excluding contributions from contrast agents. While this approach may underestimate the total energy deposited in contrast-enhanced scans, it reflects the biologically relevant dose to native tissue. Future studies may need to incorporate iodine contrast into dose calculations. Sixth, in this study, NPS was calculated using previous measured shapes derived from a homogeneous phantom and scaled by patient-specific noise estimated from patient CT images. Future work could explore alternative methods, such as using subtraction method, to estimate NPS directly from patient images. Seventh, this study focused only on individualized dose and image quality assessment. Further study is warranted to apply the methodology and data for optimization of CT devices, procedures, and protocols.

In summary, patient-specific organ-based dose and image quality were assessed in nearly 10,000 clinical CT cases using automated approaches. The results demonstrate the clinical feasibility of the patient-specific organ-based approach and show that non-organ-based metrics cannot fully represent individualized metrics of quality and safety.

Table 2
Median and 75th percentile of effective dose based on organ dose (E_{OD}) for chest-abdomin-pelvis exams (a) and E_{OD} for abdomen-pelvis exams (b) and *in vivo* model observer detectability (d′) for both chest-abdomen-pelvis and abdomen-pelvis exams (c).

(a) E_OD for chest-abdomin-pelvis

	21–24.9 cm		25–28.9 cm		29–32.9 cm		33–36.9 cm		37–40.9 cm			All sizes	
Exam group	50th	75th	50th	75th	50th	75th	50th	75th	50th	75th	P Value	50th	75th
VA T1	6.4	6.4	9.7	11.9	13.2	14.4	12.8	14	10.5	11	<0.001	12.3	13.8
VA T2	4.9	5.9	6.5	8.3	9.8	11.6	11.6	12.3	12.2	12.2	<0.001	9.3	11.6
VA T3							16	17.9	13.8	14.4	0.4	14.9	16.3
VA T4							14.4	15.4	16	16.4	0.8	15.2	16.4
VA T5	6	6.1	6.5	7.3	8.8	10	12.1	13.1	12.6	16.5	<0.001	9	11.5
VA T6	6	6.1	6.6	7.1	9	10.4	12.4	13.7	13.3	14.4	<0.001	9.5	11.6
VA T7	5.6	5.9	5.7	6.1	7.4	8.4	10.1	10.9	12.4	14.4	<0.001	7.3	9.2
VA T8							12.8	14.5	13.8	16.2	0.2	13.4	15.2
VA T9	3.9	4	5	5.5	6.9	7.9	9.2	10.8	12	12.3	<0.001	6.9	8.5
VA T10	3.3	3.5	5.1	5.4	7	7.9	8.8	9.7	7.2	8	<0.001	7	8.3
VB T1	3.9	4.1	4.6	5.2	5.2	5.8	5.7	6.3	6	6.6	<0.001	5.1	5.8
VB T2													
VB T3													
VB T4			6.5	7.1	8	9	8.1	10.8	8.3	8.9	<0.001	8.1	9.6
VB T5	5.3	5.6	5.9	6.4	6.4	6.9	6.9	7.5	7.5	8.2	<0.001	6.4	6.9
VB T6			9.8	11	10.3	11.3	10.6	15.8	10.9	12	0.6	10.8	12.2
VB T7					9.6	9.6	10.1	11.1	11	11.7	0.2	10.7	11.4
VB T8	5	5.4	5.2	6	5.9	6.9					<0.001	5.6	6.4
VB T9	5.9	6	6.4	6.8	6.9	7.8	7.2	8	7.6	7.6	<0.001	6.8	7.7
VB T10			7	7	7.7	8.3	7.6	8			0.3	7.6	8.1
All	5.3	5.8	5.7	6.5	6.7	8.3	8.3	11.5	11.1	13	<0.001	6.6	8.6

b. E_OD for abdomen-pelvis exams

	21–24.9 cm		25–28.9 cm		29–32.9 cm		33–36.9 cm		37–40.9 cm			All sizes	
Exam group	50th	75th	50th	75th	50th	75th	50th	75th	50th	75th	P Value	50th	75th
VA T1	4.1	4.3	5.9	6.7	8.6	9.5	9.3	10.1	7.6	8.4	<0.001	8.1	9.3
VA T2	2.7	2.9	4.4	5.1	6.7	7.5	8.4	9.2	8.2	10.2	<0.001	6.3	7.9
VA T3					10.5	10.5	12.2	13.4	10.8	12.2	<0.001	11	13.1
VA T4					8.6	9.3	11.5	11.8	11.1	12.5	0.2	10.9	11.9
VA T5	3.7	4.1	4.1	4.9	6.5	7.5	9	10.1	9.8	11.2	<0.001	6.5	8.4
VA T6	4	4.5	4.2	4.5	6.5	8	9.1	10.3	9	10.9	<0.001	7.3	9
VA T7	3.6	4	3.6	4	5.1	5.9	7.8	8.8	8.7	9	<0.001	5	7
VA T8							9.4	10.7	10.5	12.5	0.2	10.1	11.1
VA T9	2.9	3.1	2.8	2.9	4	4.8	6	6.8	7.5	7.5	<0.001	4.2	5.4
VA T10	2.1	2.1	3	3.6	4.5	5.4	6.3	7.1	6.3	6.3	<0.001	4.3	5.7
VB T1	2.5	2.6	3.2	3.6	3.7	4.2	4.4	5	4.7	5.5	<0.001	3.7	4.4
VB T2			3.4	3.7	4.1	4.6	4.6	5.1	5	5.7	<0.001	4.4	5.1
VB T3	3.7	4.1	4.3	4.7	4.8	5.5	5.3	5.8	5.5	5.6	<0.001	4.7	5.4
VB T4			4.9	5	5.2	5.4	6.9	7.7	6.6	7.1	<0.001	6.5	7.4
VB T5	3.8	3.9	4.2	4.6	4.8	5.3	5.5	6	5.9	6.5	<0.001	4.7	5.4
VB T6							8.7	9.5	8.5	10	0.8	8.6	9.9
VB T7					9.7	9.7	8.3	8.7	8.6	10.4	0.2	8.4	9.4
VB T8	3	3.2	3.7	4	3.9	4.3	4.2	4.3			<0.001	3.7	4.2
VB T9	4.1	4.1	4.7	5.3	5.2	5.5	5.8	6.2	5.4	5.7	0.1	5.1	5.7
VB T10			4.5	4.5	5.9	6.5	5.7	7	6.5	6.9	0.6	5.9	6.9
All	3.5	4	4.3	5	5.4	7.1	7.3	9.1	7.9	10.4	<0.001	5.4	7.5

(c) d′ for all exams

	21–24.9 cm		25–28.9 cm		29–32.9 cm		33–36.9 cm		37–40.9 cm			All sizes	
Exam group	50th	75th	50th	75th	50th	75th	50th	75th	50th	75th	P Value	50th	75th
VA T1	1.2	1.2	1.2	1.3	1.3	1.3	1.2	1.3	1.1	1.2	<0.001	1.2	1.3
VA T2	1.4	1.5	1.4	1.5	1.5	1.6	1.6	1.7	1.6	1.8	<0.001	1.5	1.6
VA T3					1.5	1.5	1.4	1.5	1.3	1.4	0.001	1.3	1.5
VA T4					1.6	1.6	1.9	2.1	1.9	2.1	0.144	1.9	2
VA T5	1.9	2.1	1.6	1.7	1.7	1.9	2	2.2	2	2.1	<0.001	1.8	2
VA T6	2.5	2.7	2.4	2.8	2.9	3.2	3.4	3.6	3.3	3.5	<0.001	3	3.4
VA T7	2.3	2.5	2	2.1	2	2.2	2.4	2.6	2.6	2.9	<0.001	2.1	2.4
VA T8							2.2	2.3	2.3	2.4	0.369	2.2	2.3
VA T9	2.1	2.1	2.1	2.2	2.4	2.7	2.6	2.7	2.5	2.5	<0.001	2.4	2.6
VA T10	2.7	2.8	3.1	3.3	3.3	3.5	3.3	3.5	3	3	<0.001	3.2	3.4
VB T1	1.6	1.7	1.4	1.6	1.3	1.4	1.2	1.3	1.1	1.2	<0.001	1.3	1.5
VB T2			1.7	2	1.6	1.7	1.6	1.7	1.4	1.4	<0.001	1.6	1.7
VB T3	2.4	2.6	2.1	2.3	2	2.2	1.8	1.9	1.5	1.6	<0.001	1.9	2.2
VB T4			1.7	1.8	1.6	1.7	1.4	1.5	1.3	1.5	<0.001	1.4	1.6
VB T5	2.1	2.4	1.9	2.1	1.8	1.9	1.6	1.7	1.3	1.5	<0.001	1.7	2
VB T6			2.1	2.1	1.9	1.9	1.6	1.8	1.4	1.6	<0.001	1.5	1.7
VB T7					2	2	1.9	2	1.7	1.9	0.318	1.7	2
VB T8	1.3	1.4	1.2	1.4	1.2	1.3	1.3	1.4			0.54	1.2	1.4

(*continued on next page*)

Table 2 (*continued*)

(c) d' for all exams

	21–24.9 cm		25–28.9 cm		29–32.9 cm		33–36.9 cm		37–40.9 cm			All sizes	
Exam group	50th	75th	50th	75th	50th	75th	50th	75th	50th	75th	P Value	50th	75th
VB T9	1.5	1.5	1.3	1.5	1.2	1.3	1.1	1.2	1	1.1	0.003	1.2	1.4
VB T10			1.5	1.7	1.3	1.5	1.2	1.3	1	1.1	<0.001	1.2	1.4
All	1.7	2.3	1.6	2	1.6	1.9	1.6	2	1.5	1.9	<0.001	1.6	2

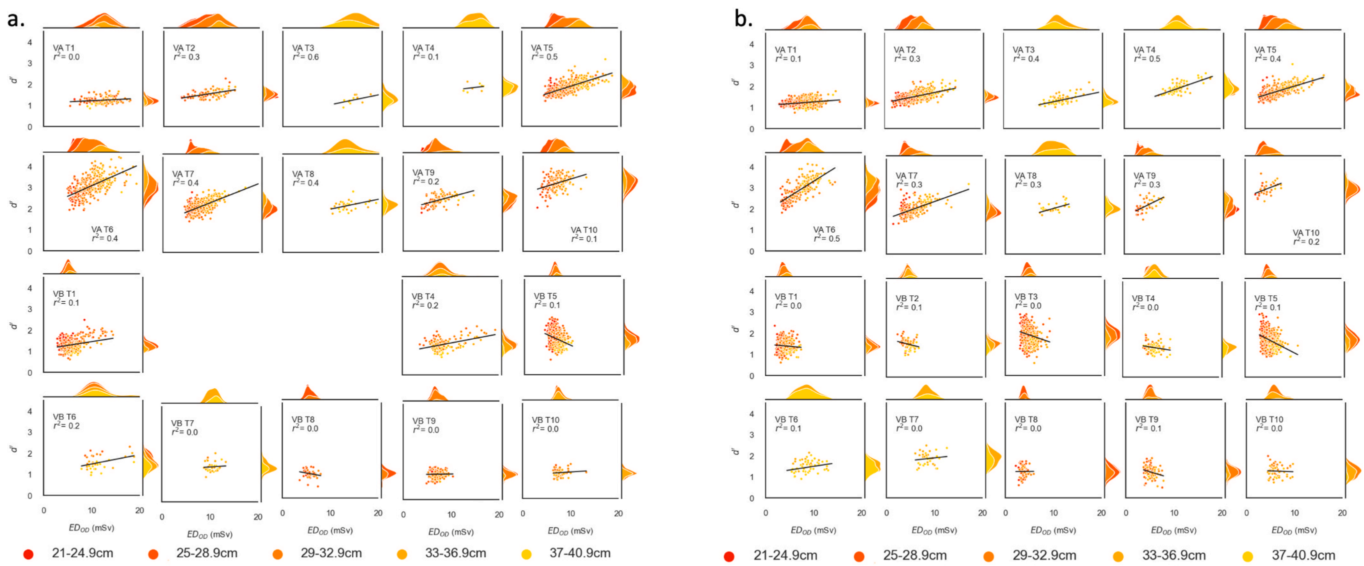

Fig. 4. Scatterplots of detectability (d') vs. effective dose based on organ dose E_{OD} with their histograms on the margins for *chest-abdomen-pelvis exams* (a) and for *abdomen-pelvis exams* (b). Each subplot shows exams with scan parameters VA T1 to VB T10 (VA or VB represent vendors; T represents techniques). Different colors represent different water equivalent diameter ranges. Each data point is one exam measurement plotted with linear regression line (black solid line). Note the empty plots indicate no exams were found for the specific scan settings.

Further, the results show varied relationships between dose and image quality in actual patient cases, which implies imaging optimization is best done at a personalized level and semi-independently.

Declaration of competing interest

The authors declare the following financial interests/personal relationships which may be considered as potential competing interests: Ehsan Samei discloses relationship with the following entities unrelated to the present publication: GE, Siemens, Imalogix, 12Sigma, SunNuclear, Nanox, Metis Health Analytics, Cambridge University Press, and Wiley and Sons. Other authors disclose no relationship relevant to this paper.

Acknowledgement

This work was supported in part by a program project grant from the NIH (P41EB028744).

References

[1] Brenner DJ, Hall EJ. Computed tomography — an increasing source of radiation exposure. N Engl J Med 2007;357:2277–84.
[2] Jaffe TA, Yoshizumi TT, Toncheva G, et al. Radiation dose for body CT protocols: variability of scanners at one institution. Am J Roentgenol 2009;193:1141–7.
[3] McCollough CH, Chen GH, Kalender W, et al. Achieving routine submillisievert CT scanning: report from the summit on management of radiation dose in CT. Radiology 2012;264:567–80.
[4] Boone JM, Hendee WR, McNitt-Gray MF, Seltzer SE. Radiation exposure from CT scans: how to close our knowledge gaps, monitor and safeguard exposure—proceedings and recommendations of the radiation dose summit, sponsored by NIBIB, February 24–25, 2011. Radiology 2012;265:544–54.
[5] Li X, Samei E, Segars WP, Sturgeon GM, Colsher JG, Frush DP. Patient-specific radiation dose and cancer risk for pediatric chest CT. Radiology 2011;259:862–74.
[6] Boone J, Strauss K, Cody D et al (2011) AAPM report No. 204: size-specific dose estimates (SSDE) in pediatric and adult body CT examinations. American Association of Physicists in Medicine website.
[7] McCollough C, Bakalyar DM, Bostani M, et al. Use of water equivalent diameter for calculating patient size and size-specific dose estimates (SSDE) in CT: the report of AAPM task group 220. AAPM Report 2014;2014:6.
[8] Hardy AJ, Bostani M, Kim GHJ, Cagnon CH, Zankl MA, McNitt-Gray M. Evaluating size-specific dose estimate (SSDE) as an estimate of organ doses from routine CT exams derived from Monte Carlo simulations. Med Phys 2021.
[9] Valentin J. Managing patient dose in multi-detector computed tomography (MDCT). Elsevier New York; 2007.
[10] Samei E, Tian X, Segars WP. Determining organ dose: the holy grail. Pediatr Radiol 2014;44:460–7.
[11] Samei E, Pawlicki T, Bourland D, et al. Redefining and reinvigorating the role of physics in clinical medicine: a report from the AAPM medical physics 3.0 ad hoc committee. Med Phys 2018;45:e783–9.
[12] Publ I. 2007 recommendations of the international commission on radiological protection. Ann ICRP 2008;37:2–4.
[13] Vañó E, Miller D, Martin C, et al. Diagnostic reference levels in medical imaging. ICRP publication 135. Ann ICRP 2017;46:1–144.
[14] Vennart W (1997) ICRU Report 54: Medical imaging-the assessment of image quality-ISBN 0-913394-53-X. April 1996, Maryland, USA. Radiography 3:243-244.
[15] Smith TB, Solomon JB, Samei E. Estimating detectability index in vivo: development and validation of an automated methodology. J Med Imaging 2017;5:031403.
[16] Fu W, Sharma S, Abadi E, et al. iPhantom: a framework for automated creation of individualized computational phantoms and its application to CT organ dosimetry. IEEE J Biomed Health Inform 2021.
[17] Çiçek Ö, Abdulkadir A, Lienkamp SS, Brox T, Ronneberger O (2016) 3D U-Net: learning dense volumetric segmentation from sparse annotationInternational conference on medical image computing and computer-assisted intervention. Springer, pp 424-432.
[18] Avants BB, Tustison NJ, Song G, Cook PA, Klein A, Gee JC. A reproducible evaluation of ANTs similarity metric performance in brain image registration. Neuroimage 2011;54:2033–44.

[19] Sharma S, Kapadia A, Fu W, Abadi E, Segars WP, Samei E. A real-time Monte Carlo tool for individualized dose estimations in clinical CT. Phys Med Biol 2019;64:215020.
[20] Jadick G, Abadi E, Harrawood B, Sharma S, Segars WP, Samei E. A scanner-specific framework for simulating CT images with tube current modulation. Phys Med Biol 2021;66:185010.
[21] Protection R. ICRP publication 103. Ann ICRP 2007;37:2.
[22] Fu W, Sharma S, Smith T et al (2019) Multi-organ segmentation in clinical-computed tomography for patient-specific image quality and dose metrologyMedical Imaging 2019: Physics of Medical Imaging. International Society for Optics and Photonics, pp 1094829.
[23] Christianson O, Winslow J, Frush DP, Samei E. Automated technique to measure noise in clinical CT examinations. Am J Roentgenol 2015;205:W93–9.
[24] Chen B, Christianson O, Wilson JM, Samei E. Assessment of volumetric noise and resolution performance for linear and nonlinear CT reconstruction methods. Med Phys 2014;41:071909.
[25] Sanders J, Hurwitz L, Samei E. Patient-specific quantification of image quality: an automated method for measuring spatial resolution in clinical CT images. Med Phys 2016;43:5330–8.
[26] Kanal KM, Butler PF, Sengupta D, Bhargavan-Chatfield M, Coombs LP, Morin RL. US diagnostic reference levels and achievable doses for 10 adult CT examinations. Radiology 2017;284:120–33.
[27] Haji-Momenian S, Ellenbogen A, Khati N, et al. Comparing dose-length product–based and Monte Carlo simulation organ–based calculations of effective dose in 16-and 64-MDCT examinations using automatic tube current modulation. Am J Roentgenol 2018;210:583–92.
[28] Fu W, Ria F, Segars WP, et al. Patient-informed organ dose estimation in clinical ct: implementation and effective dose assessment in 1048 clinical patients. Am J Roentgenol 2021;216:824–34.
[29] Siegel MJ, Schmidt B, Bradley D, Suess C, Hildebolt C. Radiation dose and image quality in pediatric CT: effect of technical factors and phantom size and shape. Radiology 2004;233:515–22.
[30] Ria F, Jadick G, Abadi E, Solomon JB, Samei E. Comparing two different noise magnitude estimation methods in CT using virtual imaging trialsMedical imaging 2022. Physics of Medical Imaging. International Society for Optics and Photonics. 2022.
[31] Mazloumi M, Van Gompel G, Kersemans V, de Mey J, Buls N. The presence of contrast agent increases organ radiation dose in contrast-enhanced CT. Eur Radiol 2021;31:7540–9.